DOI: 10.1002/cssc.201000377

Improved Niobate Nanoscroll Photocatalysts for Partial Water Splitting

Troy K. Townsend,[a] Erwin M. Sabio,[a] Nigel D. Browning,[b, c] and Frank E. Osterloh*[a]

Layered $K_4Nb_6O_{17}$ is a known UV-light-driven photocatalyst for overall water splitting, with a band gap of 3.5 eV. Following ion exchange and exfoliation with tetrabutylammonium hydroxide, the layered material separates into nanosheets that coil into 1.0 ± 0.5 μm long and 10 ± 5 nm wide nanoscrolls to reduce their surface energy. Pt and IrO_x ($x = 1.5$–2) nanoparticles were photochemically deposited onto the surface of the nanoscrolls to produce two- and three-component photocatalysts. Under UV irradiation, the nanostructures produced H_2 from pure water and aqueous methanol, with turnover numbers ranging from 2.3 and 18.5 over a 5 h period. The activity of the catalysts for H_2 evolution can be directly correlated with the varying overpotentials for water reduction (210–325 mV). From water, no oxygen is evolved. Instead, the formation of surface-bound peroxides in a 1:1 stoichiometry with H_2 is observed. Slow photochemical oxygen evolution can be achieved with the sacrificial electron acceptor $AgNO_3$, and under an electrochemical bias. The electrochemical water oxidation overpotentials are ca. 600 mV across the series of scrolls. From the photo onset potential the conduction band edge for the unmodified scrolls is estimated as −0.75 V at pH 7. Deposition of a co-catalyst is found to depress this value by 58 mV (IrO_x), 148 mV (Pt/IrO_x), and 242 mV (Pt). However, because water oxidation remains rate-limiting, this does not affect the overall performance of the catalysts.

Introduction

Developing a cheap and active water splitting photocatalyst for solar fuel collection may be one of the most important challenges of the century. Given that sunlight and water are practically infinite sources of fuel, solar hydrogen from semiconductor photocatalysts is expected to be the most promising solution to the global energy dilemma.[1] Currently, however, no economically competitive water-splitting photocatalyst has been realized, mainly due to the low efficiency of the conversion process and limited visible light absorption. Nanomaterials, as catalysts, offer potential advantages with higher catalytic surface area and shorter pathways for charge and exciton transport compared to bulk materials. These properties have led to the successful application of nanoscale Fe_2O_3 as a photoanode material.[2] Nanocrystals also exhibit quantum size effects, which allow controllable adjustment of energy levels and light absorption. Nanoscale CdSe is an active photocatalyst, for example, while bulk CdSe is not.[3,4] A problem with nanocrystals is that space charge layers, if present at all, are not strong enough to enable efficient electron–hole separation. Potentially this problem can be solved with co-catalysts, which can act as selective electron or hole acceptors. However, the optimization of such contacts is a challenge because data on the energetic structure of nanomaterials and composites are still scarce. Besides, there are synthetic obstacles for the preparation of defined multicomponent nanostructures. As part of our ongoing search for a nanoscale water-splitting photocatalyst,[3–13] we describe here scalable syntheses of catalysts that contain up to three separate nanoparticle components for light absorption, water reduction, and oxidation. The light absorber is a niobate nanoscroll derived by chemical exfoliation from the known water-splitting photocatalyst $K_4Nb_6O_{17}$.[14–17] The asymmetrical scroll structure of this material is thought to enhance charge separation. To introduce sites for water reduction and oxidation, Pt and IrO_x ($x = 1.5$–2) nanoparticle co-catalysts are attached to the nanoscrolls by photochemical deposition. The morphology, optical, electrochemical, photocatalytic, and energetic properties of these nanomaterials are reported here.

Results and Discussion

The synthetic steps involved in the formation of the niobate nanoscrolls and the addition of the Pt and IrO_x co-catalysts are shown in Scheme 1. Sequential treatment of $K_4Nb_6O_{17}$ with dilute acid and with tetrabutylammonium hydroxide leads to the exfoliation of individual niobate layers, which then turn

[a] T. K. Townsend, E. M. Sabio, Prof. F. E. Osterloh
Department of Chemistry
University of California, Davis
One Shields Avenue, Davis, CA 95616 (USA)
Fax:(+1) 530 752 8995
E-mail: fosterloh@ucdavis.edu

[b] Prof. N. D. Browning
Department of Chemical Engineering and Materials Science
University of California, Davis
One Shields Avenue, Davis, CA 95616 (USA)

[c] Prof. N. D. Browning
Lawrence Livermore National Laboratory
7000 East Avenue, Livermore, CA 94550 (USA)

Supporting Information for this article is available on the WWW under http://dx.doi.org/10.1002/cssc.201000377.

 © 2011 Wiley-VCH Verlag GmbH & Co. KGaA, Weinheim

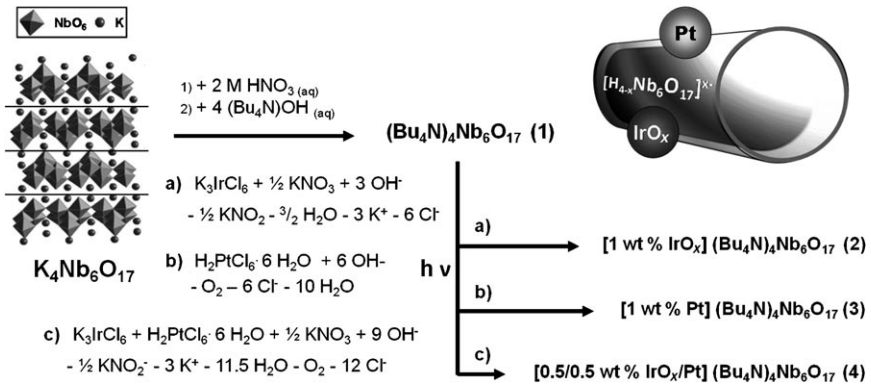

Scheme 1. Synthesis of nanocrystal photocatalysts. The structure of $K_4Nb_6O_{17}$ (including exfoliation lines) and the schematic structure of the nanoscrolls with co-catalysts is also shown.

into scrolls (**1**) because of the inherent strain of the asymmetrical structure.[17] By irradiating a mixture of the scrolls (**1**) together with potassium hexachloroiridate (III) and nitrate as electron acceptor, one obtains the IrO_x-modified scrolls **2**. Scrolls coated with platinum nanoparticles (**3**) can be obtained similarly, by photochemical deposition using a mixture of **1** and hexachloroplatinic acid. Pt/IrO_x-modified scrolls **4** were produced by sequential deposition of first Pt and then IrO_x, or by co-deposition, using a mixture of the Pt and Ir reagents. Products of the aqueous syntheses were isolated as wet solids by using precipitation and centrifugation steps, as described in the Experimental Section.

Transmission electron microscopy (TEM) images confirm the expected morphology of products **1**-**4**. Niobate scrolls (**1**) are 1 ± 0.5 μm long and 10 ± 5 nm wide (Figure 1a and b), in agreement with observations by Saupe et al.[17] The overlapping lattice fringes evident in Figure 1c and d can be related to the characteristic spacing between rows of Nb atoms.[18,19] Nanoscrolls loaded with 1 wt% Pt show discrete nanoparticles (< 2 nm) deposited on the surface (Figure 1e–h). When imaged with high-resolution scanning transmission electron microscopy (HRSTEM), the lattice fringes of the crystalline Pt particles were measured as 0.195 nm and match the known spacing of platinum for the [100] axis.[20] In contrast, the 1 wt% IrO_x nanoscrolls in Figure 1i–l showed no visible lattice fringes, indicating an amorphous deposition. IrO_x is known to form an amorphous oxide/hydroxide phase when grown in solution phase.[21] Images of the three-component catalyst containing 0.5 wt% Pt and 0.5 wt% IrO_x (Figure 1m–p) share features of the two-component structures, displaying discrete crystalline Pt particles and amorphous IrO_x regions. The co-catalysts could also be directly identified by energy-dispersive spectroscopy (EDS, see Figure S1 in the Supporting Information). Regioselective deposition was observed on the asymmetric nanoscroll, with Pt growing predominately on the edges of the rolled crystal sheets whereas IrO_x deposition appeared to have no selectivity.

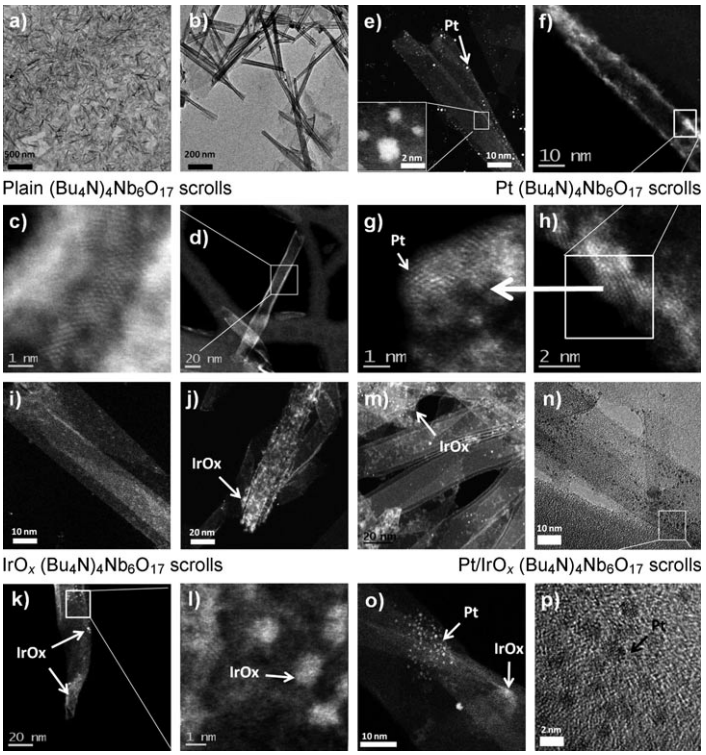

Figure 1. a,b) TEM, c–m, o) high-angle annular dark field scanning TEM (HAADFSTEM), and n, p) high-resolution TEM images of $(Bu_4N)_4Nb_6O_{17}$ nanoscrolls (a–d), Pt nanoscrolls (e–h), IrO_x nanoscrolls (i–l), and Pt/IrO_x nanoscrolls (m–p).

UV/Vis spectra (Figure 2) show the optical absorption edge of $K_4Nb_6O_{17}$ (348 nm), corresponding to the 3.55 eV band gap of the parent material. For the exfoliated $(Bu_4N)_4Nb_6O_{17}$ nanoscrolls the absorption onset is shifted to 375 nm, corresponding to a reduced band gap of 3.3 eV. We have previously attributed this band gap reduction to weakening of Nb–O bonds due to bending in the nanoscrolls.[9] After Pt and/or IrO_x deposition, the samples become colored (see photographs in Figure 2). The platinum-coated scrolls appear brown due to broad visible absorption similar to that of platinum colloids.[22] The IrO_x-coated scrolls are also brown, not blue as observed for colloidal $Ir^{IV}O_2$.[23] This indicates that most of the iridium ions are in the +3 oxidation state. However, Ir^{III} oxide is also active as a water oxidation catalyst.[24,25] The scrolls containing both platinum and IrO_x share optical characteristics of the scrolls loaded with either platinum or IrO_x.

Photoirradiation experiments with the nanoscroll catalysts were conducted over 5 h periods in aqueous methanol (20 vol%), 25 mM aqueous silver nitrate solution, and in pure water, using 100 mg (ca. 120 μmol) of catalyst in each case.

 © 2011 Wiley-VCH Verlag GmbH & Co. KGaA, Weinheim

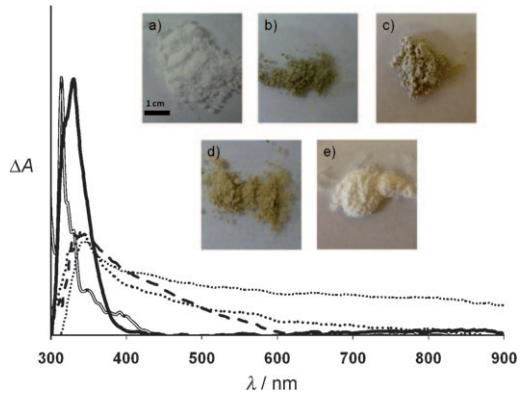

Figure 2. Diffuse reflectance UV/Vis spectra of the four catalysts and the parent material. Open line: $K_4Nb_6O_{17}$ bulk (a), small-dotted line: Pt/IrO_x $(Bu_4N)_4Nb_6O_{17}$ (b), dotted line: Pt $(Bu_4N)_4Nb_6O_{17}$ (c), dashed line: IrO_x $(Bu_4N)_4Nb_6O_{17}$ (d), solid line: $(Bu_4N)_4Nb_6O_{17}$ (e). The photographs show coloration due to co-catalyst deposition.

From methanol solution, all catalysts evolve H_2 at a constant rate. [Pt]$(Bu_4N)_4Nb_6O_{17}$ (**3**) is most active (ca. 500 μmol h^{-1}), followed by [IrO_x,Pt]-$(Bu_4N)_4Nb_6O_{17}$ (**4**, ca. 250 μmol h^{-1}), $(Bu_4N)_4Nb_6O_{17}$ (**1**), and [IrOx]$(Bu_4N)_4Nb_6O_{17}$ (**2**). The latter evolve H_2 at nearly the same rate of ca. 100 μmol h^{-1}. Turnover numbers range between 4.9 (for **1**) to 18.5 (for **3**), establishing a catalytic process (Table 1).

From water the catalysts evolve H_2, but the rates are only about half of those in aqueous methanol. The relative activities of the four catalysts are the same as in aqueous methanol, with [IrO_x]$(Bu_4N)_4Nb_6O_{17}$ (**2**) being the least active material. Importantly, we find that in water, H_2 evolution can not be sustained and in the case of the most active catalyst **3** drops to nearly zero after 24 h of continuous irradiation (Figure 3 d). This deactivation can be attributed to coating of the nanosheet surface with peroxides, as we have previously demonstrated for nanosheets of the related phase $HCa_2Nb_3O_{10}$.[8] The latter catalyze the splitting of water into hydrogen and Nb(5+)-bound η^2-peroxide. Indeed, titration of post-irradiated platinated scrolls (**3**) with the indicator *o*-tolidine (details in the Supporting Information) reveals that peroxides are also present in a 1:1 ratio with regard to the amount of released H_2 (Figure 3 d). This confirms that the diminishing reactivity of the scrolls must be due to peroxide poisoning. Assuming that each of the six niobium ions in the scrolls can accommodate one peroxide ligand, the scrolls can release at most six mole equivalents of hydrogen. This is exactly what is observed for **3** in Figure 3 d, after replacement of residual tetrabutylammonium (TBA) surfactant with protons via repeated precipitation/washing steps. Under these conditions 120 μmol of $H_4Nb_6O_{17}$ (100 mg) evolve up to 680 μmol of H_2 over a 24 h period, that is, $H_2/H_4Nb_6O_{17} = 5.7$. In the presence of TBA, the amount of H_2

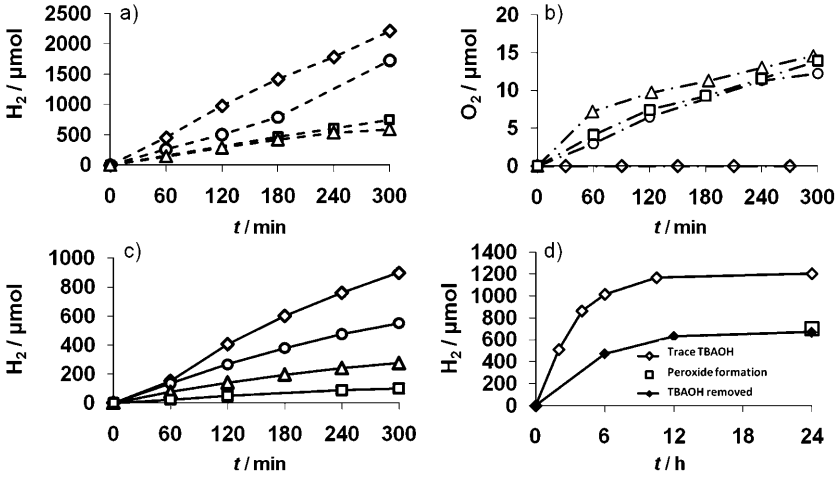

Figure 3. H_2 and O_2 evolution under UV irradiation with a 300 W Xe arc lamp from 100 mg of catalyst suspended in 50 mL of a) 20 % aqueous methanol, b) pure water, and c) 25 mM aqueous $AgNO_3$. Diamonds: Pt nanoscrolls, circles: Pt/IrO_x nanoscrolls, triangles: $(Bu_4N)_4Nb_6O_{17}$ nanoscrolls, squares: IrO_x nanoscrolls. d) Hydrogen evolution during long term (24 h) irradiation of 100 mg 1 % Pt nanoscrolls (**3**) in water. Also shown in the plot is H_2 evolution data for **3** after removal of residual tetrabutyl ammonium hydroxide (TBAOH), and the amount of peroxide detected coulometrically via reaction with *o*-tolidine (for details, see Figure S2 in the Supporting Information).

Table 1. Catalyst turnover numbers, calculated as moles of formed H_2/O_2 per mole of $H_4Nb_6O_{17}$ catalyst (molecular mass 834 g mol^{-1}, 120 μmol for 100 mg) after 5 h of irradiation.

$H_4Nb_6O_{17}$ nanoscroll catalyst	Solution		
	pure water	methanol (20 vol %)	$AgNO_3$ (25 mM)
Unmodified	2.3	4.9	0.1
IrO_x	0.8	6.24	0.1
Pt	8.3	18.5	0.0
Pt/IrO_x	4.6	14.4	0.1

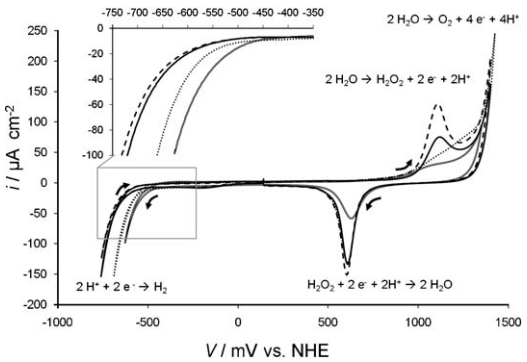

Figure 4. Cyclic voltammograms of films of the four catalysts on a Au electrode (1 cm^2) in 0.25 M NaH_2PO_4/Na_2HPO_4 buffer at pH 7 and scan rate of 10 mV s^{-1}. Open line: Pt nanoscrolls, dotted line: Pt/IrO_x nanoscrolls, solid line: $(Bu_4N)_4Nb_6O_{17}$ nanoscrolls, dashed line: IrO_x nanoscrolls. The arrows show the scan direction. All potentials are given vs. NHE. Additional scans on bare Pt and Au electrodes (Figure S3 in Supporting Information) show that background currents from the Au electrode can be neglected.

 © 2011 Wiley-VCH Verlag GmbH & Co. KGaA, Weinheim

from irradiation in water is higher (see Figure 3d and Table 1). We attribute this to side reactions of the peroxide with the tetrabutylammonium ion, as previously described for TBA-$Ca_2Nb_3O_{10}$ nanosheets.[8]

Problems with O_2 evolution persist even when catalysts are irradiated in the presence of 25 mM $AgNO_3$ as sacrificial electron acceptor (Figure 3b). Only noncatalytic amounts of O_2 are formed, or none as in the case of [Pt]$(Bu_4N)_4Nb_6O_{17}$. The O_2 evolution rate declines over time, in part due to peroxide poisoning of the catalyst, and also as a result of Ag particle deposition onto the scrolls.

Further insight into the differences in catalytic activity of these nanocomposites can be obtained using cyclic voltammetry (Figure 4). Cathodic scans reveal significant differences of 0.21–0.325 V between the actual and theoretical reduction potential for water (−410 mV vs. NHE at pH 7). The 1% Pt nanoscrolls (**3**) showed the lowest reduction overpotential (0.21 V), as expected. For the remaining catalysts, cathodic overpotentials increase in the order Pt/IrO_x (**4**) < nanoscroll (**1**) < IrO_x (**2**). This parallels the order of activity for H_2 evolution rates in both water and in aqueous methanol. Figure 5 is a plot of the rates of H_2 evolution for these systems against the electrochemical overpotentials. The data can be fit to a straight line in both

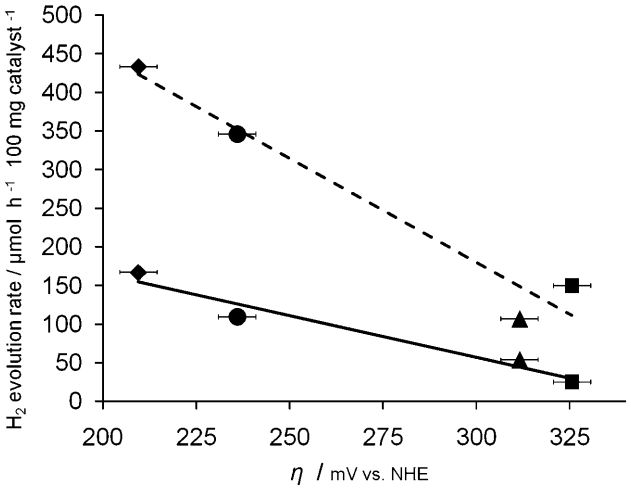

Figure 5. Correlation between measured reduction overpotentials and photocatalytic H_2 evolution rate. Dashed line: aqueous methanol (20 vol%), solid line: pure water. Diamonds: Pt nanoscrolls, circles: Pt/IrO_x nanoscrolls, triangles: $(Bu_4N)_4Nb_6O_{17}$ nanoscrolls, squares: IrO_x nanoscrolls. Error bars correspond to 10% experimental error.

cases, but the slope is larger in methanol than in water. This makes sense because methanol oxidation is less difficult than water oxidation, so that the proton reduction rate becomes the limiting factor. In the absence of methanol, water oxidation becomes the rate limiting step, based on the lower H_2 evolution rates from water in Figure 3, however H_2 reduction still has an effect on the overall rate.

Electrochemically, water oxidation is observed for all materials significantly above the theoretical potential (+820 mV vs. NHE at pH 7). The first oxidation wave at +1.10 belongs to the two-electron oxidation of water to peroxide as shown in Figure 4, with a corresponding reduction process on the reverse scan occurring at +600 mV. The shapes and potentials of these redox features are very similar to gold electrodes, after correcting for the difference in pH.[26,27] Indeed, if the nanoscroll film is kept at 1.2 V NHE bias for 1 h, peroxides can be directly detected on the surface using a peroxidase-coated test strip (Figure S4). Peroxide formation is favored energetically because of the strong binding affinity to Nb(5+) and kinetically, because it involves fewer redox steps and fewer reactive intermediates in comparison to O_2 formation. For the Pt-containing materials, water oxidation to peroxide is observed as only a shoulder, which could indicate a fast follow up reaction, for example, the Pt-catalyzed peroxide disproportionation into O_2 and H_2O. This reaction is not complete, however, because the peroxide reduction peak at +600 mV can still be observed, albeit at lower amplitude for the scrolls **3** with the largest Pt loading. The electrochemical properties of the IrO_x-loaded scrolls, on the other hand, are nearly identical to the unloaded scrolls. This means that water oxidation proceeds mainly on the niobate and that the IrO_x particles merely assume a spectator role.

The second oxidation peak at > 1400 mV corresponds to the formation of O_2, which can be seen directly as gas bubbles at the electrode. This process occurs at roughly the same potential for all catalysts, indicating that O_2 evolution takes place directly on the nanoscroll surface, not on the co-catalysts. The IrO_x co-catalysts do not improve the situation because their mass fraction in **2** is small, and because there appears to be no efficient pathway for hole transport from the nanoscrolls to the IrO_x particles. Also, the photodeposited brown IrO_x is known to be not as active for water oxidation as the blue IrO_2.[24,25] The fact that the O_2 evolution overpotential (ca. 600 mV) is 2 to 3 times the value of the proton reduction overpotential (210–325 mV) clearly shows that oxygen evolution is the limiting factor in photocatalytic water splitting with these materials.

In addition to the potential scans in water, we also performed voltammetry scans under chopped illumination and in the presence of methanol as electron donor (Figure 6a). These scans serve to determine the onset potential for the anodic photocurrent, which can be used to estimate the conduction band edge in highly n-doped metal oxide semiconductors.[28–30] One can see that at pH 7, the sizes of the photocurrents differs among catalysts, with the strongest currents observed for [Pt]-$(Bu_4N)_4Nb_6O_{17}$ (**3**). Onset potentials are observed from −0.50 to −0.80 V. Together with the optical bandgaps, this data was used to construct the energy diagrams in Figure 6b. The figure shows that the conduction bands of all nanoscrolls are above the proton reduction potential in neutral solution (−410 mV vs. NHE). The co-catalysts are found to depress the conduction band edge by 58 mV (IrO_x), 148 mV (Pt/IrO_x), and 242 mV (Pt) in positive direction from the value for the unmodified scrolls (−748 mV). This observation compares well with our previous electrochemical studies on platinum-modified $H_2Ti_4O_9$ nanocrystals.[13] The shift can be interpreted as a result of electron

 © 2011 Wiley-VCH Verlag GmbH & Co. KGaA, Weinheim

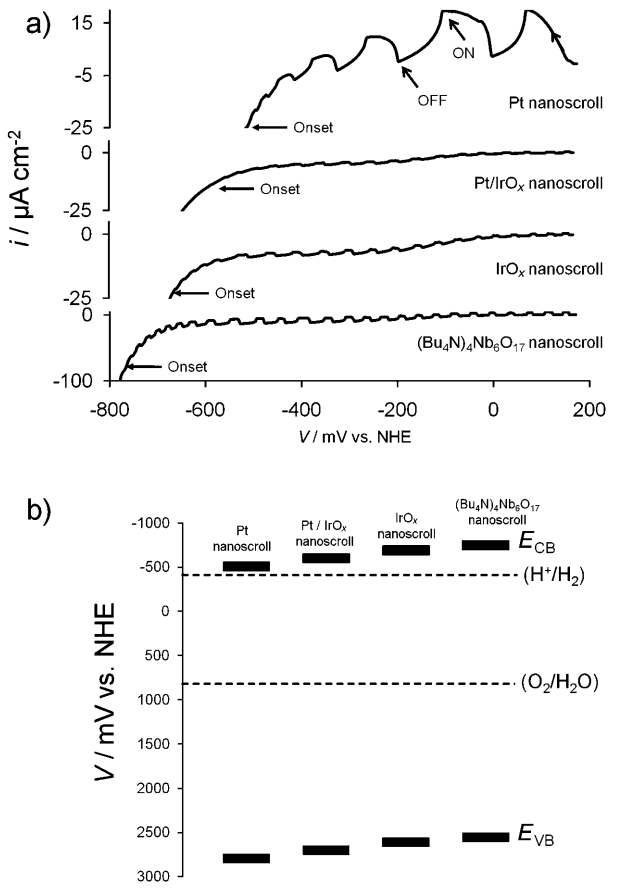

Figure 6. a) Reduction scans (10 mV s^{-1}) of catalysts deposited and dried as a thin film onto a gold 1 cm^2 electrode in 25 mM NaH_2PO_4 pH 7 buffer with chopped light, and b) resulting energy band diagrams of each catalyst.

transfer from the niobate to the co-catalysts, in the direction of lower Fermi energy. The effect is so pronounced in these systems because of the large interfacial area between the nanoscrolls and the co-catalyst particles. One might expect that the associated polarization should lessen the thermodynamic driving force for water reduction, thereby reducing the H_2 evolution rate. However, this is not observed here, because the photocatalytic H_2 activity in methanol solution is not controlled by the energetics of the catalysts but by the kinetics of proton reduction (electrochemical overpotentials). For water oxidation the situation is similar. Even though the valence band edges of all catalysts are well below the water oxidation potential, oxygen formation is inhibited kinetically due to the large overpotential for its formation and to the greater ease of peroxide formation on the niobate surface.

Conclusions

We have synthesized Pt- and/or IrO_x-coated niobate nanoscrolls by combination of a top down (exfoliation) and a bottom-up approach (photochemical deposition). The resulting two- and three-component nanostructures are catalytically active for photochemical H_2 evolution from aqueous methanol, but they evolve only limited amounts of H_2 from water, and non-stoichometric amounts of O_2 from aqueous $AgNO_3$ solution. In methanol, the H_2 evolution rates are inversely correlated with H^+ overpotentials, which shows that the process is limited by the rate of proton reduction. In water and aqueous silver nitrate, oxygen evolution is strongly retarded because of a large kinetic barrier for O_2 formation (the electrochemical overpotential is 2–3 times as large as the H_2 overpotential) and due to the strong binding affinity of peroxide to Nb(5+). The formation of niobate-bound peroxides is the reason for the diminishing hydrogen evolution activity in water. This reaction is not prevented by the Pt and IrO_x co-catalysts. We also find that the co-catalysts depress the niobate conduction band energy, based on the photo-onset potentials. However, in the presence of the other limiting factors, this does not affect the activity of the catalysts.

Experimental Section

Reagents. K_2CO_3, Nb_2O_5, and TBA(OH) (40 wt% in H_2O) were purchased from Acros Organics and used Scheme 1. $H_2PtCl_6{\cdot}6H_2O$, K_3IrCl_6, H_2SO_4, and HNO_3 (70%) were purchased from Sigma–Aldrich. KNO_3 and $AgNO_3$ were obtained from Fisher Scientific, Pittsburgh, PA. Reagents were of reagent quality and were used as received. Water was purified to >18 MΩcm resistivity using a Nanopure system. $K_4Nb_6O_{17}$ was prepared according to a literature method.[14]

$(Bu_4N)_4[Nb_6O_{17}]$ scrolls (1). The scrolls were prepared as described previously.[17] Initially, an acid treatment of 2.0 g (1.93 mmol) bulk $K_4Nb_6O_{17}{\cdot}3H_2O$ powder with 250 mL of 2 M HNO_3 was carried out for 5 days. The resulting white product was centrifuged and washed four times with 50 mL of pure water. Exfoliation of the wet acid exchange product involved adding TBA hydroxide (40 wt% in water, Acros) in a 20:1 molar ratio (26.6 mL, 40.5 mmol) and stirring for 5 days. This white solution was centrifuged and washed twice with pure water. During the second wash, the precipitate was discarded and the supernatant (containing a homogeneous colloid suspension of nanoscrolls) was isolated for the following study. The concentration of the colloid was measured gravimetrically to be 10 mg mL^{-1} which corresponds to an average total of 1.0 g $(Bu_4N)_4[Nb_6O_{17}]$ (28% yield, $M = 1798$ g mol^{-1}). Transmission electron microscopy (TEM) reveals thin sheets that have rolled into a rod-like structure with multiple layers.

[Pt, IrOx, and Pt/IrOx] $(Bu_4N)_4[Nb_6O_{17}]$ scrolls (2,3,4). Platinum nanoparticles were deposited onto the surface of the niobate scrolls by adding 2.13 mg H_2PtCl_6 (85 wt% in water, Acros) to a dispersion of 100 mg of niobate scrolls in 50 mL of water. The solution was purged with Ar gas and irradiated under UV light for 1 h with a Xe arc lamp. The colored product **3** (Figure 2) was precipitated with 0.1 M H_2SO_4, washed twice with 50 mL of pure water and then redispersed in 0.5 wt% tetrabutylammonium hydroxide in water. Bright-field TEM images revealed the Pt nanoparticles as dark spots (2–3 nm in diameter) containing the characteristic lattice fringes of platinum.[20] IrO_x-modified nanoscrolls (**2**) were prepared analogously, using 2.33 mg of K_3IrCl_6 (99.9% purity, Acros), and 5 mM (25.25 mg) KNO_3 for 100 mg of niobate scrolls dispersed in 50 mL of water. The nitrate is known to facilitate deposition of IrO_x.[31] Scanning TEM (STEM) images show additional broader regions of high contrast corresponding to IrO_x deposition. Nanoscrolls containing both 0.5% Pt and 0.5% IrO_x (**4**) were synthesized in two ways. Pt and IrO_x were photodeposited sequentially, with a water washing step (50 mL) after the first deposition. Alternatively,

 © 2011 Wiley-VCH Verlag GmbH & Co. KGaA, Weinheim

Pt and IrO_x were deposited simultaneously using a mixture of 1.17 mg K_3IrCl_6 and 1.07 mg H_2PtCl_6 in 50 mL of 5 mM KNO_3 before washing four times with 50 mL of water. The two products were found to be identical in terms of their morphology and their optical and catalytic properties.

The rate of photochemical hydrogen evolution from each catalyst was determined by irradiating 100 mg of each catalyst in 50 mL of pure water in a quartz round bottom flask with a 300 W Xe arc lamp (209 mW cm^{-2} at flask, $\lambda = 220$–380 nm, measured with GaN photodetector). The air-tight irradiation system connects a vacuum pump and a gas chromatograph (Varian 3800) with the sample flask to quantify the amount of gas evolved, using area counts of the peaks and the identity of the gas from the calibrated carrier times. Prior to irradiation, the flask was evacuated down to 5 torr (666.6 Pa) and purged with argon gas. This cycle was repeated until the chromatogram of the atmosphere above the solution indicated that the sample did not contain hydrogen, oxygen, or nitrogen. Electrochemical measurements were conducted by drying a drop of the aqueous dispersions of the catalyst under nitrogen gas onto a gold electrode (1 cm^2) and submerging the dried product into an air-tight quartz flask filled with 50 mL of 0.25 M Na_2HPO_4/NaH_2PO_4 buffer solution at pH 7, containing methanol (20 vol%) as sacrificial donor. The electrochemical cell consisted of a platinum counter electrode, the working electrode (catalyst), and a saturated calomel reference electrode connected to the cell with a KCl salt bridge. Nitrogen gas was bubbled through the electrolyte solution for 10 min prior to each experiment and remained streaming above the solution during the experiment. Photocurrents were measured by irradiation delivered via a fiber optics cable from a 300 W Xe arc lamp equipped with an IR filter. Chopped light with an irradiance of 15 mW cm^{-2} at 200–380 nm illuminated the working electrode. The system was calibrated using the redox potential of $K_4[Fe(CN)_6]$ at +0.358 V (NHE). UV/Vis diffuse reflectance spectra were taken on dried films of the catalysts by using an Ocean Optics HR2000 CG-UVNIR spectrometer and a DH2000 light source. Centrifugation was achieved with a IEC Centra CL2 centrifuge. Transmission electron images were taken with a Philips CM-12 instrument at 120 kV acceleration potential. Bright field high resolution transmission electron microscopy (BF-HRTEM) images were taken using a JEOL 2500SE 200 kV TEM. *Z*-contrast high angle annular dark field scanning TEM (HAADF-STEM) images were taken using a JEOL 2100F STEM with 200 kV field emission gun and a spherical aberration corrector.

Acknowledgement

This work was supported by grant 0829142 of the National Science Foundation (NSF) and grant FG02–03ER46057 of the US Department of Energy. T.K.T. thanks NSF for a graduate student fellowship 2010 (NSFGRFP) and his group members for advice. N.D.B. thanks the US Department of Energy for support (grant FG02–03ER46057).

Keywords: heterogeneous catalysis · hydrogen · nanoparticles · niobium · water splitting

[1] N. S. Lewis, D. G. Nocera, *Natl. Acad. Sci. USA* **2006**, *103*, 15729–15735.
[2] A. Kay, I. Cesar, M. Gratzel, *J. Am. Chem. Soc.* **2006**, *128*, 15714–15721.
[3] F. A. Frame, E. C. Carroll, D. S. Larsen, M. S. Sarahan, N. D. Browning, F. E. Osterloh, *Chem. Commun.* **2008**, 2206–2208.
[4] F. A. Frame, F. E. Osterloh, *J. Phys. Chem. C* **2010**, *114*, 10628–10633.
[5] H. Zhou, E. M. Sabio, T. K. Townsend, T. Fan, D. Zhang, F. E. Osterloh, *Chem. Mater.* **2010**, *22*, 3362–3368.
[6] E. M. Sabio, M. Chi, N. D. Browning, F. E. Osterloh, *Langmuir* **2010**, *26*, 7254–7261.
[7] F. E. Osterloh, *Nanoparticle-Assembled Water Splitting Catalysts, in On Solar Hydrogen & Nanotechnology* (Ed.: L. Vayssieres), Wiley VCH, **2010**.
[8] O. C. Compton, F. E. Osterloh, *J. Phys. Chem. C* **2009**, *113*, 479–485.
[9] M. C. Sarahan, E. C. Carroll, M. Allen, D. S. Larsen, N. D. Browning, F. E. Osterloh, *J. Solid State Chem.* **2008**, *181*, 1678–1683.
[10] O. C. Compton, C. H. Mullet, S. Chiang, F. E. Osterloh, *J. Phys. Chem. C* **2008**, *112*, 6202–6208.
[11] E. C. Carroll, O. C. Compton, D. Madsen, D. S. Larsen, F. E. Osterloh, *J. Phys. Chem. C* **2008**, *112*, 2394–2403.
[12] O. C. Compton, E. C. Carroll, J. Y. Kim, D. S. Larsen, F. E. Osterloh, *J. Phys. Chem. C* **2007**, *111*, 14589–14592.
[13] M. R. Allen, A. Thibert, E. M. Sabio, N. D. Browning, D. S. Larsen, F. E. Osterloh, *Chem. Mater.* **2010**, *22*, 1220–1228.
[14] M. Gasperin, M. T. Lebihan, *J. Solid State Chem.* **1982**, *43*, 346–353.
[15] K. Domen, A. Kudo, M. Shibata, A. Tanaka, K. Maruya, T. Onishi, *J. Chem. Soc. Chem. Commun.* **1986**, 1706–1707.
[16] K. Sayama, A. Tanaka, K. Domen, K. Maruya, T. Onishi, *J. Phys. Chem.* **1991**, *95*, 1345–1348.
[17] G. B. Saupe, C. C. Waraksa, H.-N. Kim, Y. J. Han, D. M. Kaschak, D. M. Skinner, T. E. Mallouk, *Chem. Mater.* **2000**, *12*, 1556–1562.
[18] R. Kaito, K. Kuroda, M. Ogawa, *J. Phys. Chem. B* **2003**, *107*, 4043–4047.
[19] K. Teshima, Y. Niina, K. Yubuta, T. Suzuki, N. Ishizawa, T. Shishido, S. Oishi, *Eur. J. Inorg. Chem.* **2007**, 4687–4692.
[20] B. Y. Xia, J. N. Wang, X. X. Wang, *J. Phys. Chem. C* **2009**, *113*, 18115–18120.
[21] M. Yagi, E. Tomita, T. Kuwabara, *J. Electroanal. Chem.* **2005**, *579*, 83–88.
[22] F. Mafuné, J. Y. Kohno, Y. Takeda, T. Kondow, *J. Phys. Chem. B* **2003**, *107*, 4218–4223.
[23] P. G. Hoertz, Y. I. Kim, W. J. Youngblood, T. E. Mallouk, *J. Phys. Chem. B* **2007**, *111*, 6845–6856.
[24] G. S. Nahor, P. Hapiot, P. Neta, A. Harriman, *J. Phys. Chem.* **1991**, *95*, 616–621.
[25] A. Mills, T. Russell, *J. Chem. Soc. Faraday Trans.* **1991**, *87*, 1245–1250.
[26] I. Burke, P. Nugent, *Gold Bull.* **1997**, *30*, 43–47.
[27] D. R. Merrill, I. C. Stefan, D. A. Scherson, J. T. Mortimer, *J. Electrochem. Soc.* **2005**, *152*, E212–E221.
[28] A. J. Bard, L. R. Faulkner, *Electrochemical Methods: Fundamentals and Applications*, 2nd Ed., John Wiley, New York, **2001**, p. 754.
[29] A. Ishikawa, T. Takata, J. N. Kondo, M. Hara, H. Kobayashi, K. Domen, *J. Am. Chem. Soc.* **2002**, *124*, 13547–13553.
[30] K. Akatsuka, G. Takanashi, Y. Ebina, N. Sakai, M. Haga, T. Sasaki, *J. Phys. Chem. Solids* **2008**, *69*, 1288–1291.
[31] A. Iwase, H. Kato, A. Kudo, *Chem. Lett.* **2005**, *34*, 946–947.

Received: November 3, 2010
Published online on January 18, 2011

 © 2011 Wiley-VCH Verlag GmbH & Co. KGaA, Weinheim